The Ca 2+ -and phospholipid-binding protein Annexin A2 is able to increase and decrease plasma membrane order

Svetlana Varyukhina, Antonin Lamazière, Jean Louis Delaunay, Anaëlle de Wreede, Jesus Ayala-Sanmartin

The Ca^{2+}- and phospholipid-binding protein Annexin A2 is able to increase and decrease plasma membrane order

Svetlana Varyukhina[a], Antonin Lamazière[a], Jean Louis Delaunay[a], Anaëlle de Wreede[a] and Jesus Ayala-Sanmartin[a,b,*]

a, INSERM, Centre de Recherche Saint-Antoine (CRSA), UMR_S 938, Université Sorbonne, Paris, France.

b. CNRS, Paris, France

* Corresponding author: Centre de recherche Saint Antoine (CRSA), 27 rue Chaligny, 75012 Paris, France. Tel: +33 6 81 01 94 87. e-mail: jesus.ayala-sanmartin@sorbonne-universite.fr

Abbreviations: ANE, Di-4-ANEPPDHQ; AnxA2, annexin A2; Chol, cholesterol; GP, generalised polarization; H_{II}, inverted hexagonal phase; Ld, liquid-disordered; Lo, liquid-ordered; LUV, large unilamellar vesicle; MLV, multilamellar vesicle; PC, phosphatidylcholine; PE, phosphatidylethanolamine; PS, glycerophosphatidyl-L-serine; Q, cubic phase; SAXD, small angle x-ray diffraction; TID, 3-(trifluoromethyl)-3-(*m*[^{125}I]iodophenyl)diazirine; WT, wild type.

Abstract

Annexin A2 (AnxA2) is a calcium- and phospholipid-binding protein that plays roles in cellular processes involving membrane and cytoskeleton dynamics and is able to associate to several partner proteins. However, the principal molecular partners of AnxA2 are negatively charged phospholipids such as phosphatidylserine and phosphatidyl-inositol-(4,5)-phosphate. Herein we have studied different aspects of membrane lipid rearrangements induced by AnxA2 membrane binding. X-ray diffraction data revealed that AnxA2 has the property to stabilize lamellar structures and to block the formation of highly curved lipid phases (inverted hexagonal phase, H_{II}). By using pyrene-labelled cholesterol and the environmental probe di-4-ANEPPDHQ, we observed that in model membranes, AnxA2 is able to modify both, cholesterol distribution and lipid compaction. In epithelial cells, we observed that AnxA2 localizes to membranes of different lipid order. The protein binding to membranes resulted in both, increases and/or decreases in membrane order depending on the cellular membrane regions. Overall, AnxA2 showed the capacity to modulate plasma membrane properties by inducing lipid redistribution that may lead to an increase in order or disorder of the membranes.

Keywords: Annexin A2, cholesterol, fluorescence, membrane domains, X-ray diffraction.

1. Introduction

Cellular membranes are composed of different protein and lipid species. The current model of membrane lipid organization propose the existence of lipid affinities that result in the formation of different membrane domains with particular physicochemical properties such as lipid order, fluidity, lipid packing and diffusional rates. Different aspects of membrane domain organization, membrane asymmetry, physicochemical properties and cellular functions have been discussed in several reviews [1–8]. The role of cholesterol (Chol) as a lipid-organizing molecule is now well known. Cholesterol is able to promote lipid ordering depending on its concentration in membrane models and giant plasma membrane vesicles, as well as by molecular dynamics simulations [9–13]. Membrane domains have been classified into two groups; liquid-ordered domains (Lo) usually enriched in cholesterol and lipids with saturated acyl chains such as sphingomyelin, and liquid-disordered domains (Ld) which are enriched in lipids with unsaturated acyl chains and can be poor in cholesterol content. It has been shown that cholesterol mediated the formation of membrane domains and its increase in lipid order depended on the phospholipid head group and the saturation or unsaturation of the acyl chains [14–16]. The CH-O hydrogen bonds between cholesterol and phosphatidylcholine (PC) or sphingomyelin seem to play a crucial role in the formation of membrane micro-domains [17], and the interaction of cholesterol with different phospholipids results in different cholesterol diffusional rates [18].

The members of the annexin family of calcium- and phospholipid-binding proteins have been involved in many different cellular membrane processes (for reviews see [19,20]). In particular, annexin A2 (AnxA2) is not only able to bind to membranes, but can also form protein bridges between two membranes in its monomeric and tetrameric forms. It has been suggested that these membrane bridges play a role in membrane fusion processes. The calcium dependence of these membrane binding and bridging properties is modulated by the presence of cholesterol. This cholesterol effect was observed in model membranes and cellular membranes such as chromaffin granules [21]. Moreover, this membrane-binding modulation by cholesterol was observed for other annexins such as annexins A5, A6 and A8 in membrane models [22] and cultured cells [23,24]. AnxA2 has been found associated to cholesterol enriched membrane domains in a calcium-dependent manner in smooth muscle cells [25], and in HeLa cells' plasma membranes during entero-pathogenic *E. coli* cell attachment [26]. AnxA2 does not bind directly to cholesterol [21,27] suggesting that the cholesterol effect on AnxA2 binding is mediated by cholesterol-induced membrane domain

organization. In agreement with this suggestion, experiments with membrane models show a very complex behaviour of AnxA2 calcium dependency that depends not only on cholesterol concentration, but also on different phospholipid proportions [28]. Experiments with breast cancer cells showed that the presence of long-chain saturated fatty acids increases the translocation of AnxA2 to cholesterol-enriched, detergent-resistant membranes [29].

Other experimental data suggest that annexins are able to induce lipid segregation and micro-domain marker protein clustering in a calcium-dependent manner in smooth muscle cells, chromaffin cells and fibroblasts [30–32]. In computer simulations, annexin A5 and AnxA2 induced clusters of phosphatidylserine (PS)/cholesterol, and lipid ordering [33,34]. In planar-supported bilayers and in giant unilamellar vesicles (GUVs), AnxA2 was able to induce the formation of different domains, indicating that the protein induces lipid segregation [35,36]. AnxA2 also induced an increase in membrane order (Laurdan fluorescence shift), and phosphatidylinositol-bis-phosphate (PI(4,5)P2) clustering in GUVs. These clusters were stabilized by the presence of cholesterol [27]. Therefore, it seems that the pre-existent membrane domains modulate AnxA2 binding and, reciprocally, after membrane association, the protein induces lipid reorganization.

Herein, we studied the lipid membrane rearrangements induced by AnxA2. In model membranes, we focused the experiments on the comparison of AnxA2 effects on membranes in both, the presence and the absence of cholesterol. X-ray diffraction data showed that AnxA2 favours the lamellar structures and reduced the tendency of membranes to form highly curved structures. Experiments using fluorescent probes and large unilamellar vesicles (LUVs) indicated that the protein induced cholesterol reorganization and increased membrane fluidity. In cells, the protein seemed to modify membrane order in different plasma membrane domains. Overall, the data support that one of the most important roles of AnxA2 is to be a modulator of membrane lipid organization.

2. Materials and methods

2.1. Materials.

Egg yolk L-α-phosphatidylcholine (PC), egg yolk L-α-phosphatidylethanolamine (PE), brain L-α-glycerophosphatidyl-L-serine (PS), cholesterol and the calcium ionophore ionomycin were purchased from Sigma-Aldrich. Human recombinant AnxA2 and S100A10 were

purified as described [37]. 3-(trifluoromethyl)-3-(*m*[^{125}I]iodophenyl)diazirine ([^{125}I]TID) 9.25 MBq, was acquired from Amersham. Di-4-ANEPPDHQ (ANE) was obtained from Dr Leslie M. Loew (Connecticut, USA), and pyrene-labelled cholesterol (py-met-chol) was a kind gift of Dr. André Lopez (Toulouse, France). Goat polyclonal anti-AnxA2 (C16) was from Santa-cruz Biotechnology (Texas,USA), anti-MRP2 (Multidrug resistance-associated protein) (M2-I-4) antibody were purchased from Alexis Biochemicals (San Diego, CA). Secondary antibodies anti goat Alexa 488 and anti-mouse Alexa 555 were from Invitrogen-Life Technologies (Saint-Aubin, France) and DRAQ5 used to stain nuclei was from Cell-Signalling Technology (MA,USA).

2.2. Large unilamellar vesicles (LUV).

LUVs of varying lipid compositions were prepared by extrusion as described in [38], in the calcium buffering solution A (Hepes 40 mM, pH 7, KCl 30 mM, EGTA 1 mM). LUVs containing the two most important phospholipids of the inner leaflet of the plasma membrane (PC and PE) and the most common AnxA2 ligand phospholipid (PS), both with and without cholesterol (PC/PS/PE, 25/15/60 and PC/PS/PE/Chol, 14/10/44/32 in mole%) were prepared. For fluorescence experiments, cholesterol-pyrene probe was added at 3.6 mole%, and ANE were added at 1 µM in solution.

2.3. X-ray diffraction.

Samples for small angle X-ray diffraction (SAXD) were prepared as described in [39]. Multilamellar vesicles (MLVs) with and without cholesterol (PC/PS/PE 25/15/60 and PC/PS/PE/Chol 14/10/44/32 in mole%), and MLVs without the AnxA2 ligand PS (PC/PE/Chol 20/50/30 in mole%) were prepared. Briefly, samples were prepared by dissolving 20 mg of lipids in chloroform/methanol (2/1, vol/vol) to obtain the indicated lipid proportions. The solvent was evaporated, and traces of solvent were removed by storage under high vacuum for two days. The dry lipids were hydrated with an equal weight of buffer A and 0.1 mM Ca^{2+} containing 5 mg of AnxA2. For X-ray acquisition, lipid samples (~20 µl) were deposited between two thin mica windows and mounted on a programmable thermal stage (Linkam, UK). Increments of 2°C in temperature of the samples were raised from 15°C to 45°C before being decreased to 20°C. Temperature was monitored by a thermocouple (Quad Service, Poissy, France) inserted directly into the lipid dispersion. Samples were exposed to the beam (1.5 Å wavelength) for 30 seconds. The SAXD quadrant detector response was corrected for the uneven channel response using a static radioactive iron, and

was calibrated for d-spacing using hydrated rat-tail collagen. The analysis of diffractogram peaks were performed with the programs Origin60 and PeakFit v4.

2.4. Cell culture and transfection.

MDCK (kidney) and HepG2 (hepatic) epithelial cell lines expressing AnxA2-GFP (green fluorescent protein; GFP) chimaera were used. The AnxA2-GFP expression vector was a kind gift from Dr Stephen Moss (London UK, [40]. MDCK and HepG2 cells were transfected by the standard lipofectamine (Thermo Fisher) protocol. Stable cell lines were obtained by selection of transfected cultures with neomycin during 10 days. The cells were cultured as previously described [41]. Briefly, cells were incubated in Dulbecco's Modified Eagle's Medium (DMEM; Life Technologies, France) supplemented with 10% heat-inactivated foetal bovine serum (Life Technologies), penicillin (0.1 IU/ml) and streptomycin (100 mg/ml). Cells were grown at 37°C in a 5% CO_2/air atmosphere. µ-slide 8 well slides from Ibidi were used for live-cell di-4-ANEPPDHQ imaging.

2.5. Cell labelling and fluorescence microscopy.

For di-4-ANEPPDHQ (ANE) labelling, the probe was added at a final 5 µM concentration for 20 minutes and then ANE was washed out. We followed the protocol previously published [42]. Briefly, confocal images were acquired with a TCS SP2 laser-scanning spectral system (Leica, Wetzlar, Germany) attached to a Leica DMR inverted microscope. For ANE imaging, the samples were excited at 488 nm (Ar ion laser) and the fluorescence emission was collected at 570-590 nm for the liquid-ordered (Lo) contribution and at 620-640 nm for the liquid-disordered (Ld) contribution. Imaging of AnxA2-GFP was performed by excitation at 488 nm and the emission light was collected at 500-520 nm. With these range of wavelengths for each parameter (Lo, Ld, GFP) and at low sensitivity of PMTs, we avoided the contamination of GFP emission on ANE spectra. Optical sections were recorded with 63/1.4 or 100/1.4 immersion objectives. For the analysis of general polarization (GP) lipid order parameter, the images were analysed using ImageJ. Intensity images were converted into GP images and each pixel was calculated from the two ANE fluorescence intensity images according to the equation:

$$GP = (I_{(570\text{-}590)} - GI_{(620\text{-}640)}) / (I_{(570\text{-}590)} + 2GI_{(620\text{-}640)})$$

Where I are the pixel intensities corresponding to the ordered (570-590) and disordered (620-640) components and G is the correction factor accounting for the instrumental difference in transmission of the $I_{(570-590)}$ and $I_{(620-640)}$ components.

GP distributions were obtained from the GP images' histogram values from regions of interest (ROI) (free plasma membranes, cell-contacting membranes and canalicular membranes) using a custom-built macro in ImageJ [30,43]. For comparison of different cell culture fields, we normalised the GP distributions in percentage considering the maximum as 100%. Pixel-by-pixel correlation of AnxA2-GFP intensity and membrane GP values was performed by quantifying the pixel values of GP, and the AnxA2-GFP fluorescence intensity with ImageJ software.

For statistical purposes, we analysed different cell culture fields by acquisition of 4 to 6 confocal planes containing several cells. For each confocal plane, the regions of interest (ROIs: free, junctional or canalicular membranes) were analysed pixel by pixel (GP values and AnxA2-GFP intensity). For comparison, the AnxA2-GFP levels were normalized in %. The results of all the planes of each cell culture field were summed. These last values were considered as one experimental point (n=1). Notice that all data were obtained from three independent cell cultures.

For immunofluorescence, HepG2 cells were fixed in cold Methanol (-20°C) for 1min and co stained with Goat polyclonal anti-AnxA2 (C16) and mouse monoclonal anti-MRP2 (M2-I-4), followed by secondary antibodies anti goat Alexa 488 and anti-mouse Alexa 555, nuclei were stained with DRAQ5.

2.6. Fluorescence spectroscopy.

Spectra were obtained with a Varian fluorimeter. The cholesterol-pyrene (py-met-chol) probe emission spectra were recorded from 360 to 600 nm using a 335 nm excitation wavelength. Excitation and emission band-passes were set at 5 nm. 250 µl of buffer A at a 500 µM calcium concentration containing 5 µg of py-met-chol-labelled LUVs were added to a quartz cell. Temperature was regulated with a Peltier device. 5 µg of AnxA2 were added (protein/lipid molar ratio 1/20) and after 7 minutes, spectra were recorded. To characterize py-met-chol movements and its environment, we followed the wavelengths recommended in [44]. Briefly, 474 nm to characterize the py-met-chol aggregation (excimers) normalized by the iso-emissive point 432 (474/432), and the 373/379 (Lo/Ld) ratio. 373 nm is a marker of

liquid-ordered (Lo) domain environment around the py-met-chol, and 379 nm is a marker of liquid-disordered (Ld) environment [44].

For ANE fluorescence, the probe was used at 1 μM. Ca^{2+} was added to 200 μl of LUVs for a final 500 μM concentration. Then, 10 μg of AnxA2 were added and incubated for 10 minutes. Emission spectra were recorded from 500 to 750 nm using 485 nm excitation and the wavelengths used for GP calculation were 570 and 630 nm for the ordered and disordered phases respectively. ΔGP = GP in the presence of AnxA2 and Ca^{2+} minus GP in the presence of Ca^{2+} alone.

2.7. Data analyses and statistics.

The principal component analysis (PCA) of normalized spectra treated as a multivariate (wavelength) set of data was performed with SIMCA software (Umetrics) as previously described [44]. Briefly, the program finds the components (correlated set of variables) that are responsible for the optimal separation of experimental observations in a multivariate space. Both, principal components analysis (PCA) and orthogonal partial least square-discriminant analysis (OPLS-DA) were performed. Different tools of the program SIMCA were used to evaluate the discriminant variables. The variable importance of the projection (VIP) summarises the importance of variables to explain X (wavelengths) and correlate to Y (experimental conditions) in the projection plane, and group-to-group comparisons show the determinant variables differentiating two groups.

The mean GP distributions were analysed with GraphPad-Prism, and the peaks values were obtained with the PeakFit program using the EMG+GMG fitting curve. The student t tests were performed to analyse the TID labelling experiments (two tailed, unpaired) and py-met-chol spectral analysis (two tailed, paired) with GraphPad-Prism. Graphs are given as means ± standard error.

3. Results

3.1. AnxA2 membrane lipids rearrangements by small angle X-ray diffraction (SAXD).

X-ray diffraction is a particularly powerful technique to study lipid membrane phases [46–48]. Therefore, we followed changes in membrane lipid arrangements after AnxA2 membrane association by X-ray diffraction. Three different membranes were tested: a membrane without

AnxA2 phospholipid ligand as a negative control (PC/PE/Chol), a membrane without cholesterol (PC/PS/PE), and a membrane containing cholesterol (PC/PS/PE/Chol).

PC/PE/Chol multilamellar vesicles (MLVs) analyses at 15°C, showed diffractograms composed of two lamellar phases (Fig. 1A). By heating the sample at 45°C we observed a shift (0.26 nm) in the d-spacing of one lamellar phase indicating that it was quite fluid in nature (liquid-disordered Ld). The d-spacings are shown in table S1. The second lamellar phase showed only a very small temperature-driven shift (0.06 nm) indicating a more ordered (Lo) nature. This Lo lamellar phase is the result of the presence of cholesterol and saturated acyl chains on MLVs. The emergence of an inverted hexagonal phase (H_{II}) by heating was also observed. This is due to the high propensity of PE to form the H_{II} phase [47,48]. Lowering the temperature demonstrated the reversibility of lipid organisation. In the presence of AnxA2, we observed no changes in the number of membrane phases, and only minor changes in the d-spacing of the lamellar phases at all temperatures, confirming the absence of AnxA2 binding without PS (Fig. 1A and table S1).

The PC/PS/PE diffractograms revealed three lamellar phases at 15°C. At high temperatures (45°C), a H_{II} phase was also present (Fig. 1B). The binding of AnxA2 to these membranes results in the detection of two lamellar phases and two peaks that are likely the contribution of one cubic phase (Q). Briefly, AnxA2 stabilized lamellar phases and one cubic phase but blocked the formation of the H_{II} phase. The rise of the cubic phase in the presence of AnxA2 could be due to phase separation creating a zone rich in PE, which is able to form the cubic structure but unable to form the hexagonal phase. Because cubic phases are thought to be intermediates between lamellar and hexagonal phases [49], the AnxA2 effect could be due to the blockage of the Q-H_{II} transition. This AnxA2-induced behaviour was quite stable and the diffractograms were very similar at all temperatures. This result suggests that AnxA2 blocks strong negative curved structures.

The presence of cholesterol in MLVs (PC/PS/PE/Chol) results in a complex diffractogram. At 15°C, two lamellar phases coexist with at least one cubic phase (Fig. 1C). The temperature induces the emergence of an additional H_{II} phase. This increase in membrane heterogeneity compared with the membranes without cholesterol illustrates cholesterol's capacity to induce membrane domain separation in agreement with its lipid de-mixing properties [9–13]. The binding of AnxA2 reduced the intensity of the Q phase, conserved the two lamellar phases and blocked the formation of the H_{II} phase. This blockage of the hexagonal phase was similar to the AnxA2 effect on PC/PS/PE MLVs. A summary of SAXD experiments is shown in Fig.

1D. Briefly, AnxA2 blocked the H_{II} phase both with and without cholesterol revealing its capacity to flatten the membrane. However, the protein increased the intensity of cubic phase in the absence of cholesterol and decreased it in the presence of cholesterol. All these effects are probably due to a protein-induced modulation of the redistribution of PE, which is a lipid that induce membrane negative curvature.

3.2. Cholesterol redistribution and membrane order changes by AnxA2.

The influence of AnxA2 on cholesterol movements was studied by characterization of the pyrene-labelled cholesterol probe py-met-chol which has been successfully used to study lipoprotein-mediated cholesterol trafficking [50]. The lateral distribution and self-association of the probe is essentially due to its cholesterol moiety [51,52]. In previous studies, we succeed defining the specific wavelengths to characterize the liquid-ordered and liquid-disordered environments of py-met-chol (373 and 379 nm, respectively) [44,53]. The more accurate parameters to study cholesterol distribution are: 474/432 nm ratio, which corresponds to the pyrene excimers signal (cholesterol multimers) normalized to the iso-emissive point, and the ratio 373/379, which characterize the balance between ordered and disordered environments. We compared the AnxA2 effect on PC/PS/PE and PC/PS/PE/Chol LUVs at 37°C. Representative spectra are shown in Fig. S1A-D. In the absence of AnxA2, Ca^{2+} did not change the spectra significantly and conversely in the absence of Ca^{2+}, AnxA2 showed no effect. Fig 2A shows that py-met-chol aggregation decreases upon AnxA2 addition on both membranes. AnxA2 also showed an effect on py-met-chol environment. The protein induced a global increase of the probe's Lo environment and this increase was stronger for the PC/PS/PE/Chol membranes (difference between control and AnxA2 of 0.88 compared to the 0.028 difference between control and PC/PS/PE membranes Fig 2B). Very similar behaviour was also observed at 20°C (Fig. S1E,F) indicating that the protein conserve its ability to redistribute lipids in less fluid membranes. These data suggest that AnxA2 increases the proportion of Lo domains in model membranes (Lo/Ld increase) resulting in dilution of the labelled cholesterol probe and therefore in reduction of the excimer signal (474/432) as previously demonstrated [44,53]. Overall, the py-met-chol experiments show that AnxA2 induces cholesterol redistribution in model membranes.

In a second series of experiments we studied the action of AnxA2 on membrane order (fluidity) by using the environmental probe Di-4-ANEPPDHQ (ANE) which is able to

differentiate the Lo and Ld membranes [54,55]. This probe is sensitive to the cholesterol membrane content [56] and its spectral properties are not modified by peptide insertion into the membranes [57]. We prepared PC/PS/PE and PC/PS/PE/Chol LUVs in the presence of the probe (1 µM). We performed fluorescence experiments in the presence and absence of calcium and AnxA2 and calculated the GP parameter. AnxA2 alone showed no effect on ANE spectra. On the contrary, Ca^{2+} showed a slight change in the GP parameter (ΔGP about 0.02, increase in order). Therefore we compared the GP values of LUVs in the presence of Ca^{2+} and AnxA2 with those in the presence of Ca^{2+} alone (ΔGP = GP in the presence of AnxA2 and Ca^{2+} minus GP in the presence of Ca^{2+}) at 37°C. Fig. 2C shows that AnxA2 is able to increase significantly the order of LUVs membranes without cholesterol. Overall, these experiments show that AnxA2 is able to change membrane fluidity and cholesterol reorganisation in membrane models.

3.3. Membrane order and AnxA2 localization in living cells.

The environmental probe Di-4-ANEPPDHQ (ANE) has been used recently in the study of membrane organization in animal and plant cells [30,58–61]. Herein, we performed a series of experiments to verify that the spectral properties of fluorophores were adapted to the simultaneous capture of three signals by confocal microscopy: AnxA2 intensity and localization (AnxA2-GFP) and plasma membrane order (Lo and Ld contributions from ANE). Fig. S2A shows the fluorescent spectra of both probes. To avoid light contamination of different channels, we used the band ranges 500-520 nm for the AnxA2-GFP signal, 570-590 nm for ANE Lo and 620-640 nm for ANE Ld contributions. We adjusted the laser intensity and the PMT sensitivities to obtain specific signals. Fig. S2B presents different control experiments that show no passage of GFP fluorescent light into Lo and Ld channels and, inversely, no passage of ANE fluorescence into GFP channel. Therefore, we used these parameters to simultaneously observe the localisation of AnxA2-GFP and the Lo and Ld contributions of the probe ANE in living cells membranes.

3.3.1. Membrane order and AnxA2 in MDCK cells.

In a first series of experiments, we characterized membrane order (GP values) in MDCK cells. The cells were cultured for two days at low and intermediate densities to obtain cell

aggregates of different sizes permitting the quantification of two different plasma membrane regions of interest: membranes contacting only the culture medium (called “free membranes” here) and the plasma membranes forming part of cell-cell contacts (called “junctions” here). We analysed 24 different cell culture fields containing several cells and from four to six confocal sections. For statistics, the data from the confocal sections for each cell culture field were summed and considered as an experiment. Firstly, we compared the GP distribution of free membranes and junctions. As shown in Fig. 3D,E, the GP distribution of free membranes presented a peak at 0.09 ± 0.01 (mean ± SEM), and for the junctional membranes, at 0.03 ± 0.01 (mean ± SEM). These data show that in these conditions, free membranes are more ordered than the membranes involved in cell-cell contacts.

Differences in the plasma membrane associated AnxA2-GFP intensity were observed. As shown in Fig. 3C, the free membranes express less AnxA2-GFP (blue and cyan) than the junctional membranes (green and red). This was expected because the junctional membranes are composed of two membranes from two adjacent cells. Notice also that in the microscopy images, free membranes show a stronger Lo character than the junctional membranes (green and blue respectively in Fig 3B). The difference in membrane order measured by the GP parameter does not depend on the membrane quantity (a ratio-metric parameter) but only on the lipid order of the environment of the probe. Therefore, the difference in membrane order (GP) between the free membranes and the junctional membranes is not due to the fact that the junctions are composed of two adjacent plasma membranes. In order to find out whether there exists a preference of AnxA2 for a specific membrane order (GP value) in a particular membrane region, we characterized the correlation of AnxA2-GFP intensity and GP value pixel-by-pixel. AnxA2-GFP distribution intensity as a function of GP for both membranes shows that the maximal AnxA2-GFP intensity is close to the GP values corresponding to the maxima of GP distributions. For free membranes, AnxA2-GFP distribution was quite homogeneous in the GP range from -0.05 to 0.25, covering the whole peak of GP values (Fig. 3F). On the contrary, for junctional membranes the AnxA2-GFP is enriched in the left part of the GP peak (-0.1 to 0.05) indicating that in junctional membranes, AnxA2 has a relative preference for less ordered domains (Fig. 3G). This is illustrated in Figs 3B and C in which the junctional membranes, indicated by arrows, show more AnxA2 (red in Fig 3C) in the less ordered membrane (blue) in Fig 3B). Careful examination of the AnxA2-GFP intensity distribution suggest an AnxA2 small preference for three GP values in free membranes and two GP values for junctional membranes (Fig. 3F,G). The strongest AnxA2 expression in free

membranes were at -0.023, 0.092 and 0.225 GP values and at 0.002 and 0.058 in junctional membranes (stars in Fig. 3F,G). Therefore, AnxA2 seems to show small preferences for some GP values in the membrane surfaces in MDCK cells.

3.3.2. Membrane order and AnxA2 in HepG2 cells.

In a second series of experiments, we characterized membrane GP values in HepG2 cell line. Cells were cultured at low densities to obtain cell aggregates permitting the quantification of three different regions of interest, the free membranes, the junctional membranes and the canalicular membranes, which correspond to the apical membranes in epithelial cells. In our culture conditions, HepG2 cells were fully differentiated as shown by the presence of clear canaliculi expressing the apical transporter MRP2 (Fig. 4). The WT cells showed no AnxA2 expression at the level of the "free" plasma membrane, and low expression in the junctional membranes. In the canalicular membrane, a strong AnxA2 expression was observed (Fig 4A). We analysed 72 different cell culture fields from four independent experiments containing several cells and from four to six confocal sections. We compared the GP distributions of membranes in cells expressing or not expressing AnxA2-GFP. As presented in Figs. 5D-F, the GP distribution of free membranes shows a peak at 0.22±0.01. The junctional membranes show a peak at 0.18±0.01, and the canalicular membranes at 0.13±0.01. The peaks are close to each other; however, the view of the whole GP distributions revealed specific enrichments in the ordered zone for each membrane region resulting in differences in the spreading of the distributions (Fig. S3). Overall, the data reveal that in these conditions, the free membranes are more ordered than the canalicular membranes and that the junctional membranes possess an intermediate degree of order. The mean global membrane order in cells expressing the AnxA2-GFP was the same compared to WT cells (Fig. 5D-F).

The GP distributions peaks were found at 0.22±0.01 for free membranes, at 0.19±0.01 for junctional membranes, and at 0.13±0.01 for canalicular membranes. Careful examination reveals differences in the shape of the GP distributions. Overall, we observed different widths of GP distributions in cells expressing AnxA2-GFP compared to WT cells. This is shown by subtracting the WT cells distributions from AnxA2-GFP distributions (Fig. 5D-F bottom of panels). Free membranes did not show significant change in the shape of the distribution. We observed a minor thinning of GP distribution for junctional membranes, and a more pronounced thinning for canalicular membranes. This reduction in GP spreading suggests that AnxA2 is able to restrain membrane heterogeneity in canalicular membranes.

The correlation of AnxA2-GFP intensity and GP values reveals relative differences between the membranes. Free membranes distribution shows an increase of AnxA2-GFP correlated with an increase in GP values but with a small "peak" at -0.06 GP (Fig. 5G). For junctional membranes, AnxA2-GFP shows a similar tendency to increase its expression with the GP increase but shows more irregularities with a "peak" at 0.15 GP value (Fig. 5H). For canalicular membranes, the pattern of AnxA2-GFP expression was more complex. Fig 5I show a plateau-like expression with three "peaks" at -0.03, 0.02 and 0.16 GP values. To better characterize the differences of AnxA2 expression in the different membrane regions we performed multivariate principal component (PCA) and orthogonal partial least square-discriminant analyses (OPLS-DA). As shown in Fig S4A-C, the AnxA2-GFP expression in junctional membranes was relatively stronger than in free plasma membrane in GPs ranging from -0.2 to 0.3. Three zones of GPs 0.04, 0.13 and 0.22 showed the strongest relative AnxA2-GFP difference between these two membrane regions. The AnxA2-GFP relative expression for different GP values for junctional and canalicular membranes was quite similar (Fig S4D-F). Only a small increase in junctional membranes was observed in GPs 0.1 and 0.23. The most interesting differences in the relative AnxA2-GFP expression on different GP values were observed when comparing the canalicular and the free membranes (Fig 5J). In the zones of positive GPs (Lo) the AnxA2-GFP expression was quite similar, but in the zones of negative GPs (Ld), AnxA2-GFP was more expressed in the canalicular membranes showing three spots of local difference of expression (GPs -0.15, -0.02 and 0.02). Overall, these data show that AnxA-GFP 2 distributes in all the membrane regions but with different enrichment in zones of specific GP values in the three plasma membrane regions.

3.3.3. Membrane order and AnxA2 in HepG2 cells after calcium entry.

In the previous experiments, we studied cells in a "steady state". In order to investigate the changes in membrane order induced by AnxA2 movement to the plasma membrane, we treated WT and AnxA2-GFP expressing HepG2 cells with the calcium ionophore ionomycin, which induces Ca^{2+}-dependent AnxA2 membrane-binding. We followed GP distributions and AnxA2-GFP correlation before treatment (time 0) and at 10, 17, 24 and 31 minutes after ionophore addition. At time 0 we observed, as in previous experiments, that free membranes were more ordered than the canalicular membranes and that junctional membranes possess an intermediate degree of order in WT and AnxA2-GFP expressing cells. We compared the differences between the WT and AnxA2-GFP cells at different times after ionomycin treatment. After ionophore treatment, both the WT and the AnxA2-GFP free membranes

showed a decrease in membrane order. After 31 minutes of ionophore treatment, we observed that the disordering effect was smaller for AnxA2-GFP cells, probably because in this cell line, membranes are enriched in AnxA2-GFP before the addition of the ionophore (Fig S5). The ionophore induced small and non-significant changes in order of canalicular membranes. For junctional membranes, the WT cells showed a diminution in order during treatment (Fig. 6A). Compared to the WT cells, the AnxA2-GFP cells showed less pronounced diminution in order (Fig. 6B). As shown in Fig. 5E, junctional membranes from AnxA2-GFP expressing cells are less ordered than the WT cells and therefore, the increase in AnxA2 membrane binding induced by the ionophore produces a less important membrane order changes in AnxA2-GFP rich cells than in the WT cells. Overall, these data is in agreement with a modulation of membrane order by AnxA2 in living cells.

4. Discussion

AnxA2 has been involved in many cell membrane functions. Its principal properties are to bind negative phospholipids in a Ca^{2+}-dependent manner and to bridge membranes. Both properties are modulated by the lipid composition of the membrane bilayer in a very complex manner [28]. Cholesterol does not bind AnxA2 but its presence in membranes regulates the Ca^{2+} dependency for AnxA2 membrane binding and bridging which suggests that this phenomenon is due to cholesterol-mediated lipid redistribution [21,27]. Cholesterol does not seem to be the only lipid molecule that regulates AnxA2 membrane binding, but the nature of the phospholipid head group and the degree of fatty acyl chain saturation might play a role in AnxA2 translocation to detergent-resistant membranes [29]. Many experimental data suggest that, in one hand, AnxA2 membrane binding is able to induce membrane lipids redistribution, and on the other hand, that lipids organized in different domains modulate AnxA2 membrane binding and bridging [25,27,32,35]. In other words, a reciprocal regulation (“cross talk”) between AnxA2 and lipids seems to be a determinant of cell membrane organization and function.

In order to gain further insight into this reciprocal relationship, the aims of this study were twofold. First, we sought to compare the properties and effects of AnxA2 on model membranes containing some of the principal phospholipids of the plasma membrane’s inner leaflet in both, the presence and the absence of cholesterol. In order to mimic cellular

membranes, we used phospholipids of natural sources containing different molecular species. Second, we investigated the effects of AnxA2 on membrane lipid order in living cells.

To our knowledge, this is the first time that X-ray diffraction has been used to study lipids arrangements induced by annexins proteins. The SAXD experiments showed that AnxA2 has a propensity to stabilize lamellar phases to the detriment of highly curved lipid structures (hexagonal phase, H_{II}). The inner leaflet of the plasma membrane contains high concentrations of PE. This phospholipid favours the formation of negatively curved structures [47,48]. Moreover, it has been shown that the degree of PE unsaturation is important for micro-domain separation and stability [14,16]. This is in agreement with the presence of different lipid phases in the diffractograms. Without cholesterol and at low temperatures, three lamellar phases were observed, and at high temperatures, we observed the induction of a hexagonal phase. The presence of cholesterol in the membranes resulted in a more complex diffractogram with lamellar, hexagonal and cubic phases. In both membranes, AnxA2 showed the capacity to block the formation of the hexagonal phase and the reduction of the cubic phase contribution in cholesterol-containing membranes, indicating a strong stabilization of lamellar phases that does not depend on cholesterol contents.

Several recent studies have shown that annexins are able to induce membrane topological changes [62] (review in [63]). Annexins A4 and A5 are able to induce strong negative curvature in the form of membrane rolling. On the contrary, annexins A1, A2 and A6 can only stabilize membrane folding. It is interesting to note that folding is related to membrane flattening in the same way as observed when AnxA2 participate in membrane bridging [45,64]. This membrane flattening capacity of AnxA2 induced a reduction in phospholipids fluidity and is coherent with the lamellar stabilization and ordering data shown here. The observed AnxA2 lamellar stabilization of membranes by SAXD could be explained either by a simple physical blockage of curvature due to an important quantity of protein on the bilayer surface and/or by an AnxA2 mediated redistribution of lipids. Therefore, we performed experiments to study the effect of AnxA2 on the redistribution of cholesterol by using the py-met-chol probe which showed a behaviour in membranes very similar to that of cholesterol [52]. The results showed that in membranes with only 3.6 mole% of py-met-chol, and in membranes with 32 mole% chol and 3.6 mole% py-met-chol, AnxA2 was able to decrease probe self-contacts and to increase the global order of the membranes (Lo/Ld ratio). However, this increase in order was stronger for cholesterol-containing membranes. The reduction of the cholesterol-probe contacts is due to the increase in membrane ordered domains resulting in

probe dilution. The observed difference in Lo/Ld ratio between the cholesterol-free and cholesterol-containing membranes is due to the high content of cholesterol in the latter membranes. Overall, these experiments demonstrate that AnxA2 is able to induce not only membrane cholesterol reorganization but also redistribution of other lipids, as was observed in cholesterol-free membranes.

Experiments with cells in culture were designed to study the effect of AnxA2 on cell membrane order. We chose epithelial cells that show three different plasma membrane regions (free membranes, cell contact membranes and apical membranes). The membrane environmental probe di-4-ANEPPDHQ, which is sensitive to the cholesterol content of membranes and has been successfully used to differentiate Lo and Ld membranes [54,56] was used to study membrane order by the general polarization parameter (GP). However, it is important to make clear two points. Firstly, the real membrane order distributions are not the result of only two membrane domains (Lo and Ld); rather, they are the sum of the contributions of several membrane domains with different degrees of order. Secondly, for the measured GP, and as discussed by Dinic and collaborators [65], in conventional confocal microscopy, each pixel might contain a mix of Lo and Ld nano-domains.

MDCK cells expressing AnxA2-GFP showed that the plasma membrane in contact with the culture medium (free membrane) is more ordered than the lateral membranes involved in cell-cell contacts (junctional membranes). We characterized the AnxA2-GFP fluorescence intensity as a function of GP in both membranes and observed that the protein was present all over the membrane, but also that it showed discrete zones of higher intensity. We also observed that in junctional membranes, AnxA2 was slightly enriched in membranes of lower GP (less ordered).

The GP parameter was also studied in HepG2 cells transfected or not with AnxA2-GFP. These cells present a third plasma membrane region: the canalicular membrane, which is the equivalent to the apical membrane of epithelial cells. As was the case for MDCK-AnxA2-GFP cells, WT HepG2 cells' free membranes were more ordered than the junctional membranes. The canalicular membranes were found to be the least ordered of the three regions.

What is the functional meaning of this hierarchy? We are tempted to speculate that this could be related to membrane stress in cultured cells. Free membranes are more exposed to the fluctuations of culture medium, whereas the membranes involved in cell junctions are

protected by the surrounding cytosol environment, and the canalicular membranes are quite isolated and protected from the external environment by a closed cellular environment. These differences in stress exposition could result in particular requirements for membrane order and therefore varying needs for rigidity and resistance to environmental fluctuations. In HepG2 cells expressing AnxA2-GFP, this ordering hierarchy of GP distributions was conserved, but the GP distribution in AnxA2 expressing cells was thinner than that of WT HepG2 cells, especially for the canalicular membranes, suggesting that AnxA2 is able to reduce membrane heterogeneity by both, decreasing the order of strong Lo domains and increasing the order of strong Ld domains. The characterization of the correlation of AnxA2-GFP intensity as function of GP showed a global increase of AnxA2 expression in membranes of higher GP for the three membrane regions. However, as for MDCK cells, the HepG2 AnxA2-GFP distributions showed discrete "peaks" of preferential AnxA2 expression.

In the last series of experiments, we characterized membrane order after the induction of Ca^{2+} cell entry accompanied by an increase in AnxA2 membrane binding by using a calcium ionophore. In WT HepG2 cells, free and canalicular membranes showed only minor changes in GP distribution after ionophore addition. However, for junctional membranes we noticed a global decrease in membrane order induced by the ionophore. In AnxA2-GFP-expressing cells, the characterization of AnxA2-GFP fluorescence as a function of GP showed that in free and junctional membranes, the ionophore induced an increase in AnxA2 intensity as predicted by the induced Ca^{2+} cell entry. This AnxA2 increase was not observed for the canalicular membranes. This difference could be because at the steady state, the canalicular membranes present a high concentration of AnxA2, probably close to saturation of membrane sites. The GP analysis showed that, compared to the WT cells, the junctional membranes of Anx-GFP-expressing cells showed a less pronounced change in GP distribution suggesting that the AnxA2 present before ionophore addition stabilizes the junctional membranes. The fact that the ionophore induced a change in WT cells' junctional membranes GP distribution leading to a distribution very similar to that of the AnxA2-GFP-expressing cells suggests strongly that the observed differences between the two cell lines are really the result of the AnxA2-GFP overexpression. Overall, our data demonstrated the role of AnxA2 in the reduction of membrane heterogeneity and membrane disordering.

5. Conclusions

The data presented here contribute to clarify three important questions concerning the mechanistic of AnxA2 function.

1) How does AnxA2 change lipid distribution? Considering that cholesterol interacts weakly with PE but strongly with PS and PI(4,5)P2 [15] and that these cholesterol differential affinities are involved in membrane domains formation, the specific binding of AnxA2 to PS could definitely modify this interaction and impose a new lipid redistribution, as has been previously suggested [28]. Herein we demonstrate that AnxA2 induces changes in py-met-chol distribution, resulting in a diminution of cholesterol aggregation.

2) What is the impact of this lipid redistribution in membrane organization and properties? First, AnxA2 is able to change membrane order, as demonstrated by the global change in membrane Lo/Ld ratio with the py-met-chol probe, and in cultured cells, this lipid redistribution was evidenced by differences in di-4-ANEPPDHQ GP distribution between WT and AnxA2-GFP-expressing cells. Second, the SAXD diffractograms showed that AnxA2 is able to reduce the membrane's negative curvature tendency of phospholipids (essentially PE), thereby increasing the propensity to stabilize lamellar structures. The reduction in membrane curvature can be explained by both: lipid redistribution and PE dilution and or/mixing with other lipids. Third, AnxA2 is able to reduce membrane heterogeneity as indicated by SAXD (decrease of H_{II} and Q phases) and by the thinning of GP distribution on cultured cells.

3) Where does AnxA2 interact on cell membranes and what are the functional consequences? First of all, the ANE probe characterization showed that AnxA2 does not have a specific binding preference for a short-range GP value in the studied membranes (free, junctional and canalicular). Overall, AnxA2 was found in practically all GP values of the membranes, but its enrichment in some GP values was observed for the different membranes as shown by the small "peaks" protruding from the correlation of GP distributions and AnxA2 intensity. Secondly, AnxA2 seems to modify the GP differently in different membrane regions. Small changes in GP distribution were observed in free membranes, which were more pronounced in junctional membranes and stronger still in canalicular membranes. It is noteworthy that differences between AnxA2-GFP-expressing cells and WT cells demonstrate that AnxA2 is able to reduce and/or increase global membrane order, suggesting that it can increase order in very disordered membranes and also decrease order in very ordered membranes, as shown by the GP distribution thinning. The specific cellular roles of the variations in GP and AnxA2 expression are not known. However, our experiments show two interesting points. First, that the method we used is capable to show that the three membrane regions have different order

distributions and second, that the presence of Annexin A2 induces a modification of lipids distribution. Therefore, the data strongly support the function of AnxA2 as a membrane order modulatory protein with the capacity of both ordering and disordering, depending on the membrane domain and on lipid composition. In the future, new experimental approaches must be designed to confirm and characterize these roles of AnxA2 in cellular processes such as exocytosis, endocytosis and other membrane transport steps in which AnxA2 has been involved.

Author contributions

JA-S planned the experiments. SV, JLD, AW and JA-S performed experiments. SV, AL and JA-S analysed data. AL contributed essential material. JA-S wrote the paper.

Acknowledgments

André Lopez for py-met-chol probe. Cédric Tessier and Claude Wolf (CHU Saint Antoine, Paris) for their help with X-ray diffraction experiments. Stephen Moss for the AnxA2-GFP expression vector. Philippe Fontanges (Hôpital Tenon, Paris) for assistance in confocal microscopy.

Funding

This research was supported by CNRS and INSERM and did not receive any specific grant from funding agencies in the public, commercial, or not-for-profit sectors.

References

[1] R.J. Clarke, K.R. Hossain, K. Cao, Physiological roles of transverse lipid asymmetry of animal membranes, Biochimica et Biophysica Acta (BBA) - Biomembranes. 1862 (2020) 183382. https://doi.org/10.1016/j.bbamem.2020.183382.

[2] A. Kusumi, T.K. Fujiwara, T.A. Tsunoyama, R.S. Kasai, A.-A. Liu, K.M. Hirosawa, M. Kinoshita, N. Matsumori, N. Komura, H. Ando, K.G.N. Suzuki, Defining raft domains in the plasma membrane, Traffic. 21 (2020) 106–137. https://doi.org/10.1111/tra.12718.

[3] I. Levental, K.R. Levental, F.A. Heberle, Lipid Rafts: Controversies Resolved, Mysteries Remain, Trends in Cell Biology. 30 (2020) 341–353. https://doi.org/10.1016/j.tcb.2020.01.009.

[4] D. Lingwood, K. Simons, Lipid rafts as a membrane-organizing principle, Science. 327 (2010) 46–50. https://doi.org/10.1126/science.1174621.
[5] C.M. Rosetti, A. Mangiarotti, N. Wilke, Sizes of lipid domains: What do we know from artificial lipid membranes? What are the possible shared features with membrane rafts in cells?, Biochim Biophys Acta Biomembr. 1859 (2017) 789–802. https://doi.org/10.1016/j.bbamem.2017.01.030.
[6] F. Schmid, Physical mechanisms of micro- and nanodomain formation in multicomponent lipid membranes, Biochim Biophys Acta Biomembr. 1859 (2017) 509–528. https://doi.org/10.1016/j.bbamem.2016.10.021.
[7] E. Sezgin, I. Levental, S. Mayor, C. Eggeling, The mystery of membrane organization: composition, regulation and roles of lipid rafts, Nat. Rev. Mol. Cell Biol. 18 (2017) 361–374. https://doi.org/10.1038/nrm.2017.16.
[8] K. Simons, M.J. Gerl, Revitalizing membrane rafts: new tools and insights, Nat. Rev. Mol. Cell Biol. 11 (2010) 688–699. https://doi.org/10.1038/nrm2977.
[9] F. Favela-Rosales, A. Galván-Hernández, J. Hernández-Cobos, N. Kobayashi, M.D. Carbajal-Tinoco, S. Nakabayashi, I. Ortega-Blake, A molecular dynamics study proposing the existence of statistical structural heterogeneity due to chain orientation in the POPC-cholesterol bilayer, Biophys. Chem. 257 (2020) 106275. https://doi.org/10.1016/j.bpc.2019.106275.
[10] H.-J. Kaiser, D. Lingwood, I. Levental, J.L. Sampaio, L. Kalvodova, L. Rajendran, K. Simons, Order of lipid phases in model and plasma membranes, Proc. Natl. Acad. Sci. U.S.A. 106 (2009) 16645–16650. https://doi.org/10.1073/pnas.0908987106.
[11] I. Levental, F.J. Byfield, P. Chowdhury, F. Gai, T. Baumgart, P.A. Janmey, Cholesterol-dependent phase separation in cell-derived giant plasma-membrane vesicles, Biochem. J. 424 (2009) 163–167. https://doi.org/10.1042/BJ20091283.
[12] I. Levental, M. Grzybek, K. Simons, Raft domains of variable properties and compositions in plasma membrane vesicles, Proc. Natl. Acad. Sci. U.S.A. 108 (2011) 11411–11416. https://doi.org/10.1073/pnas.1105996108.
[13] J.R. Silvius, D. del Giudice, M. Lafleur, Cholesterol at Different Bilayer Concentrations Can Promote or Antagonize Lateral Segregation of Phospholipids of Differing Acyl Chain Length, Biochemistry. 35 (1996) 15198–15208. https://doi.org/10.1021/bi9615506.
[14] D. Huster, K. Arnold, K. Gawrisch, Influence of docosahexaenoic acid and cholesterol on lateral lipid organization in phospholipid mixtures, Biochemistry. 37 (1998) 17299–308.
[15] T.K.M. Nyholm, S. Jaikishan, O. Engberg, V. Hautala, J.P. Slotte, The Affinity of Sterols for Different Phospholipid Classes and Its Impact on Lateral Segregation, Biophys. J. 116 (2019) 296–307. https://doi.org/10.1016/j.bpj.2018.11.3135.
[16] S.R. Shaikh, M.R. Brzustowicz, N. Gustafson, W. Stillwell, S.R. Wassall, Monounsaturated PE does not phase-separate from the lipid raft molecules sphingomyelin and cholesterol: role for polyunsaturation?, Biochemistry. 41 (2002) 10593–10602. https://doi.org/10.1021/bi025712b.
[17] S.A. Pandit, D. Bostick, M.L. Berkowitz, Complexation of phosphatidylcholine lipids with cholesterol, Biophys. J. 86 (2004) 1345–1356. https://doi.org/10.1016/S0006-3495(04)74206-X.
[18] K. Pinkwart, F. Schneider, M. Lukoseviciute, T. Sauka-Spengler, E. Lyman, C. Eggeling, E. Sezgin, Nanoscale dynamics of cholesterol in the cell membrane, J. Biol. Chem. 294 (2019) 12599–12609. https://doi.org/10.1074/jbc.RA119.009683.
[19] V. Gerke, C.E. Creutz, S.E. Moss, Annexins: linking Ca2+ signalling to membrane dynamics, Nat Rev Mol Cell Biol. 6 (2005) 449–61.
[20] U. Rescher, V. Gerke, Annexins--unique membrane binding proteins with diverse functions, J Cell Sci. 117 (2004) 2631–9.
[21] J. Ayala-Sanmartin, J. Henry, L. Pradel, Cholesterol regulates membrane binding and aggregation by annexin 2 at submicromolar Ca(2+) concentration, Biochim Biophys Acta. 1510 (2001) 18-28.
[22] J. Ayala-Sanmartin, Cholesterol enhances phospholipid binding and aggregation of annexins by their core domain, Biochem Biophys Res Commun. 283 (2001) 72–9.

[23] I. de Diego, F. Schwartz, H. Siegfried, P. Dauterstedt, J. Heeren, U. Beisiegel, C. Enrich, T. Grewal, Cholesterol modulates the membrane binding and intracellular distribution of annexin 6, J. Biol. Chem. 277 (2002) 32187–32194. https://doi.org/10.1074/jbc.M205499200.
[24] N. Heitzig, A. Kühnl, D. Grill, K. Ludewig, S. Schloer, H.-J. Galla, T. Grewal, V. Gerke, U. Rescher, Cooperative binding promotes demand-driven recruitment of AnxA8 to cholesterol-containing membranes, Biochim Biophys Acta Mol Cell Biol Lipids. 1863 (2018) 349–358. https://doi.org/10.1016/j.bbalip.2018.01.001.
[25] E.B. Babiychuk, A. Draeger, Annexins in cell membrane dynamics. Ca(2+)-regulated association of lipid microdomains, J Cell Biol. 150 (2000) 1113–24.
[26] N. Zobiack, U. Rescher, S. Laarmann, S. Michgehl, M.A. Schmidt, V. Gerke, Cell-surface attachment of pedestal-forming enteropathogenic E. coli induces a clustering of raft components and a recruitment of annexin 2, Journal of Cell Science. 115 (2002) 91–98.
[27] N.A. Gokhale, A. Abraham, M.A. Digman, E. Gratton, W. Cho, Phosphoinositide specificity of and mechanism of lipid domain formation by annexin A2-p11 heterotetramer, J Biol Chem. 280 (2005) 42831–40.
[28] F. Illien, H.R. Piao, M. Coue, C. di Marco, J. Ayala-Sanmartin, Lipid organization regulates annexin A2 Ca(2+)-sensitivity for membrane bridging and its modulator effects on membrane fluidity, Biochimica et Biophysica Acta. 1818 (2012) 2892–900.
[29] H. Zhao, R.W. Hardy, Long-chain saturated fatty acids induce annexin II translocation to detergent-resistant membranes, Biochem. J. 381 (2004) 463–469. https://doi.org/10.1042/BJ20031083.
[30] A. Alvarez-Guaita, S. Vila de Muga, D.M. Owen, D. Williamson, A. Magenau, A. Garcia-Melero, M. Reverter, M. Hoque, R. Cairns, R. Cornely, F. Tebar, T. Grewal, K. Gaus, J. Ayala-Sanmartin, C. Enrich, C. Rentero, Evidence for annexin A6-dependent plasma membrane remodelling of lipid domains, British Journal of Pharmacology. 172 (2015) 1677–90.
[31] S. Chasserot-Golaz, N. Vitale, E. Umbrecht-Jenck, D. Knight, V. Gerke, M.F. Bader, Annexin 2 promotes the formation of lipid microdomains required for calcium-regulated exocytosis of dense-core vesicles, Mol Biol Cell. 16 (2005) 1108–19.
[32] A. Draeger, S. Wray, E.B. Babiychuk, Domain architecture of the smooth-muscle plasma membrane: regulation by annexins, Biochem. J. 387 (2005) 309–314. https://doi.org/10.1042/BJ20041363.
[33] P.F. Almeida, A. Best, A. Hinderliter, Monte Carlo simulation of protein-induced lipid demixing in a membrane with interactions derived from experiment, Biophys. J. 101 (2011) 1930–1937. https://doi.org/10.1016/j.bpj.2011.09.015.
[34] D. Hakobyan, V. Gerke, A. Heuer, Modeling of annexin A2-Membrane interactions by molecular dynamics simulations, PLoS ONE. 12 (2017) e0185440. https://doi.org/10.1371/journal.pone.0185440.
[35] P. Drücker, M. Pejic, H.-J. Galla, V. Gerke, Lipid segregation and membrane budding induced by the peripheral membrane binding protein annexin A2, J. Biol. Chem. 288 (2013) 24764–24776. https://doi.org/10.1074/jbc.M113.474023.
[36] M. Menke, V. Gerke, C. Steinem, Phosphatidylserine membrane domain clustering induced by annexin A2/S100A10 heterotetramer, Biochemistry. 44 (2005) 15296–303.
[37] J. Ayala-Sanmartin, M. Zibouche, F. Illien, M. Vincent, J. Gallay, Insight into the location and dynamics of the annexin A2 N-terminal domain during Ca(2+)-induced membrane bridging, Biochim Biophys Acta. 1778 (2008) 472–82.
[38] F. Illien, S. Finet, O. Lambert, J. Ayala-Sanmartin, Different molecular arrangements of the tetrameric annexin 2 modulate the size and dynamics of membrane aggregation, Biochimica et Biophysica Acta. 1798 (2010) 1790–1796.
[39] C. Almeida, A. Lamazière, A. Filleau, Y. Corvis, P. Espeau, J. Ayala-Sanmartin, Membrane re-arrangements and rippled phase stabilisation by the cell penetrating peptide penetratin, Biochim. Biophys. Acta. 1858 (2016) 2584–2591. https://doi.org/10.1016/j.bbamem.2016.07.012.

[40] C.J. Merrifield, U. Rescher, W. Almers, J. Proust, V. Gerke, A.S. Sechi, S.E. Moss, Annexin 2 has an essential role in actin-based macropinocytic rocketing, Current Biology. 11 (2001) 1136–1141. https://doi.org/10.1016/S0960-9822(01)00321-9.
[41] M. Zibouche, F. Illien, J. Ayala-Sanmartin, Annexin A2 expression and partners during epithelial cell differentiation, Biochem. Cell Biol. 97 (2019) 612–620. https://doi.org/10.1139/bcb-2018-0393.
[42] O. Maniti, H.R. Piao, J. Ayala-Sanmartin, Basic cell penetrating peptides induce plasma membrane positive curvature, lipid domain separation and protein redistribution, The International Journal of Biochemistry & Cell Biology. 50C (2014) 73–81.
[43] D.M. Owen, C. Rentero, A. Magenau, A. Abu-Siniyeh, K. Gaus, Quantitative imaging of membrane lipid order in cells and organisms, Nat Protoc. 7 (2011) 24–35. https://doi.org/10.1038/nprot.2011.419.
[44] C. Almeida, A.D. Wreede, A. Lamazière, J. Ayala-Sanmartin, Cholesterol-pyrene as a probe for cholesterol distribution on ordered and disordered membranes: Determination of spectral wavelengths, PLOS ONE. 13 (2018) e0201373. https://doi.org/10.1371/journal.pone.0201373.
[45] O. Lambert, N. Cavusoglu, J. Gallay, M. Vincent, J.L. Rigaud, J.P. Henry, J. Ayala-Sanmartin, Novel organisation and properties of annexin 2-membrane complexes, J Biol Chem. 279 (2004) 10872–10882.
[46] A. Lamaziere, O. Maniti, C. Wolf, O. Lambert, G. Chassaing, G. Trugnan, J. Ayala-Sanmartin, Lipid domain separation, bilayer thickening and pearling induced by the cell penetrating peptide penetratin, Biochimica et Biophysica Acta. 1798 (2010) 2223–30.
[47] R.P. Rand, N.L. Fuller, Structural dimensions and their changes in a reentrant hexagonal-lamellar transition of phospholipids, Biophys. J. 66 (1994) 2127–2138. https://doi.org/10.1016/S0006-3495(94)81008-2.
[48] C. Tessier, P. Quinn, K. Koumanov, G. Trugnan, D. Rainteau, C. Wolf, Modulation of the phase heterogeneity of aminoglycerophospholipid mixtures by sphingomyelin and monovalent cations: maintenance of the lamellar arrangement in the biological membranes, Eur. Biophys. J. 33 (2004) 513–521. https://doi.org/10.1007/s00249-004-0392-5.
[49] S.-J. Marrink, D.P. Tieleman, Molecular dynamics simulation of spontaneous membrane fusion during a cubic-hexagonal phase transition, Biophys. J. 83 (2002) 2386–2392. https://doi.org/10.1016/s0006-3495(02)75252-1.
[50] G. Gaibelet, S. Allart, F. Tercé, V. Azalbert, J. Bertrand-Michel, S. Hamdi, X. Collet, S. Orlowski, Specific cellular incorporation of a pyrene-labelled cholesterol: lipoprotein-mediated delivery toward ordered intracellular membranes, PLoS ONE. 10 (2015) e0121563. https://doi.org/10.1371/journal.pone.0121563.
[51] B. Lagane, S. Mazères, C. Le Grimellec, L. Cézanne, A. Lopez, Lateral distribution of cholesterol in membranes probed by means of a pyrene-labelled cholesterol: effects of acyl chain unsaturation, Biophys. Chem. 95 (2002) 7–22. https://doi.org/10.1016/s0301-4622(01)00235-6.
[52] L. Le Guyader, C. Le Roux, S. Mazères, H. Gaspard-Iloughmane, H. Gornitzka, C. Millot, C. Mingotaud, A. Lopez, Changes of the membrane lipid organization characterized by means of a new cholesterol-pyrene probe, Biophys. J. 93 (2007) 4462–4473. https://doi.org/10.1529/biophysj.107.112821.
[53] C. Almeida, O. Maniti, M.D. Pisa, J.-M. Swiecicki, J. Ayala-Sanmartin, Cholesterol re-organisation and lipid de-packing by arginine-rich cell penetrating peptides: Role in membrane translocation, PLOS ONE. 14 (2019) e0210985. https://doi.org/10.1371/journal.pone.0210985.
[54] L. Jin, A.C. Millard, J.P. Wuskell, X. Dong, D. Wu, H.A. Clark, L.M. Loew, Characterization and application of a new optical probe for membrane lipid domains, Biophys. J. 90 (2006) 2563–2575. https://doi.org/10.1529/biophysj.105.072884.
[55] A.S. Klymchenko, R. Kreder, Fluorescent probes for lipid rafts: from model membranes to living cells, Chem. Biol. 21 (2014) 97–113. https://doi.org/10.1016/j.chembiol.2013.11.009.

[56] M. Amaro, F. Reina, M. Hof, C. Eggeling, E. Sezgin, Laurdan and Di-4-ANEPPDHQ probe different properties of the membrane, J Phys D Appl Phys. 50 (2017) 134004. https://doi.org/10.1088/1361-6463/aa5dbc.
[57] J. Dinic, H. Biverståhl, L. Mäler, I. Parmryd, Laurdan and di-4-ANEPPDHQ do not respond to membrane-inserted peptides and are good probes for lipid packing, Biochim. Biophys. Acta. 1808 (2011) 298–306. https://doi.org/10.1016/j.bbamem.2010.10.002.
[58] P. Gerbeau-Pissot, C. Der, D. Thomas, I.-A. Anca, K. Grosjean, Y. Roche, J.-M. Perrier-Cornet, S. Mongrand, F. Simon-Plas, Modification of plasma membrane organization in tobacco cells elicited by cryptogein, Plant Physiol. 164 (2014) 273–286. https://doi.org/10.1104/pp.113.225755.
[59] P. Gerbeau-Pissot, C. Der, M. Grebe, T. Stanislas, Ratiometric Fluorescence Live Imaging Analysis of Membrane Lipid Order in Arabidopsis Mitotic Cells Using a Lipid Order-Sensitive Probe, Methods Mol. Biol. 1370 (2016) 227–239. https://doi.org/10.1007/978-1-4939-3142-2_17.
[60] E. Sezgin, F. Schneider, V. Zilles, I. Urbančič, E. Garcia, D. Waithe, A.S. Klymchenko, C. Eggeling, Polarity-Sensitive Probes for Superresolution Stimulated Emission Depletion Microscopy, Biophys. J. 113 (2017) 1321–1330. https://doi.org/10.1016/j.bpj.2017.06.050.
[61] X. Zhao, R. Li, C. Lu, F. Baluška, Y. Wan, Di-4-ANEPPDHQ, a fluorescent probe for the visualisation of membrane microdomains in living Arabidopsis thaliana cells, Plant Physiol. Biochem. 87 (2015) 53–60. https://doi.org/10.1016/j.plaphy.2014.12.015.
[62] T.L. Boye, J.C. Jeppesen, K. Maeda, W. Pezeshkian, V. Solovyeva, J. Nylandsted, A.C. Simonsen, Annexins induce curvature on free-edge membranes displaying distinct morphologies, Sci Rep. 8 (2018) 10309. https://doi.org/10.1038/s41598-018-28481-z.
[63] P.M. Bendix, A.C. Simonsen, C.D. Florentsen, S.C. Häger, A. Mularski, A.A.H. Zanjani, G. Moreno-Pescador, M.B. Klenow, S.L. Sønder, H.M. Danielsen, M.R. Arastoo, A.S. Heitmann, M.P. Pandey, F.W. Lund, C. Dias, H. Khandelia, J. Nylandsted, Interdisciplinary Synergy to Reveal Mechanisms of Annexin-Mediated Plasma Membrane Shaping and Repair, Cells. 9 (2020). https://doi.org/10.3390/cells9041029.
[64] M.B. Klenow, C. Iversen, F.W. Lund, A. Mularski, A.S. Heitmann, C. Dias, J. Nylandsted, A.C. Simonsen, Annexins A1 and A2 Accumulate and Are Immobilized at Cross-Linked Membrane–Membrane Interfaces | Biochemistry, (n.d.). https://pubs-acs-org.insb.bib.cnrs.fr/doi/10.1021/acs.biochem.1c00126 (accessed June 4, 2021).
[65] J. Dinic, P. Ashrafzadeh, I. Parmryd, Actin filaments attachment at the plasma membrane in live cells cause the formation of ordered lipid domains, Biochimica et Biophysica Acta (BBA) - Biomembranes. 1828 (2013) 1102–1111. https://doi.org/10.1016/j.bbamem.2012.12.004.

Figures legends

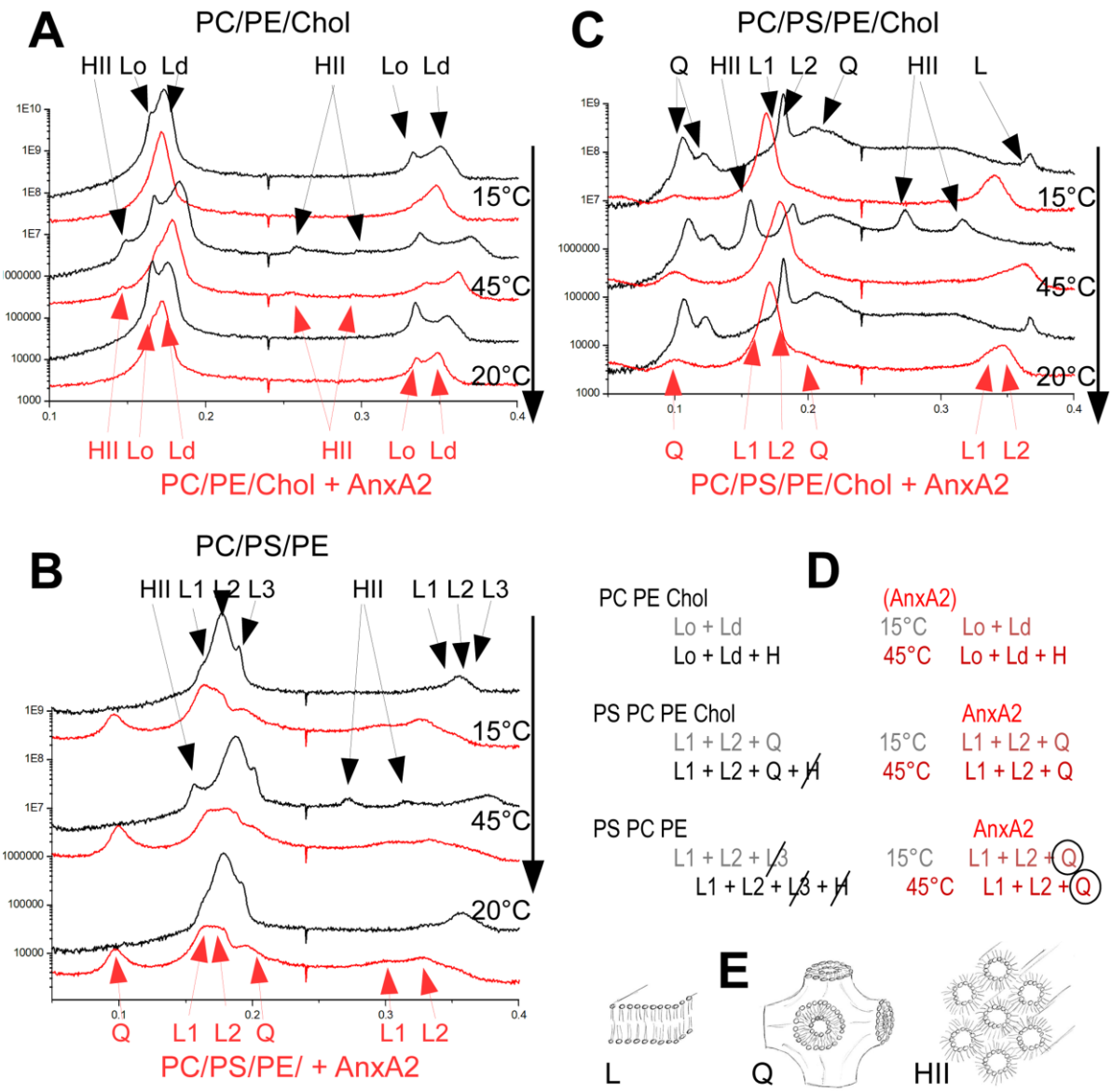

Fig. 1. Modulation of lipid organization by AnxA2. SAXD of PC/PE/Chol MLVs (A), PC/PS/PE MLVs (B) and PC/PS/PE/Chol MLVs (C). Diffractograms of MLVs alone (Black) and the in presence of AnxA2 (Red) at different temperatures during heating (top to middle) and cooling (middle to bottom). Only three temperatures are presented. Arrows indicate the position of different diffraction peaks corresponding to the first three orders of inverted hexagonal phase (H_{II}), two orders of lamellar phases (L1 or Lo and L2 or Ld) and a cubic phase (Q). D) Summary of lipid phases present in membranes (black) and the effects of AnxA2 binding (red). Light colours represent the structures at 15°C and dark colours at 45°C. The phases that disappear by the action of AnxA2 are crossed out (/) and those that appear are encircled. E) Schematic representation of the lipid phases; L, lamellar; Q, cubic; H_{II} inverted hexagonal.

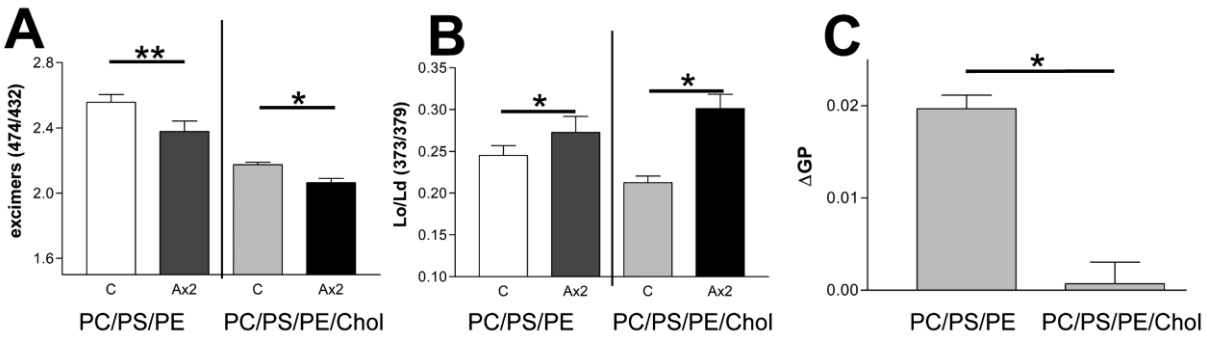

Fig. 2. AnxA2 induces lipid changes in membrane models. (A) Py-met-chol aggregation by quantification of excimers (474/432 ratio). (B), membrane order of the py-met-chol environment by quantification of the Lo/Ld ratio (373/379 nm). PC/PS/PE and PC/PS/PE/Chol LUVs were incubated at 37°C. C; LUVs alone, and Ax2; LUVs incubated with AnxA2. (C) ΔGP change of the Di-4-ANEPPDHQ fluorescence in LUVs in the presence of AnxA2 and Ca^{2+} minus in the presence of Ca^{2+}. Means ± SEM of 5 and 6 independent experiments. * P<0.05, ** P<0.01 by student t test.

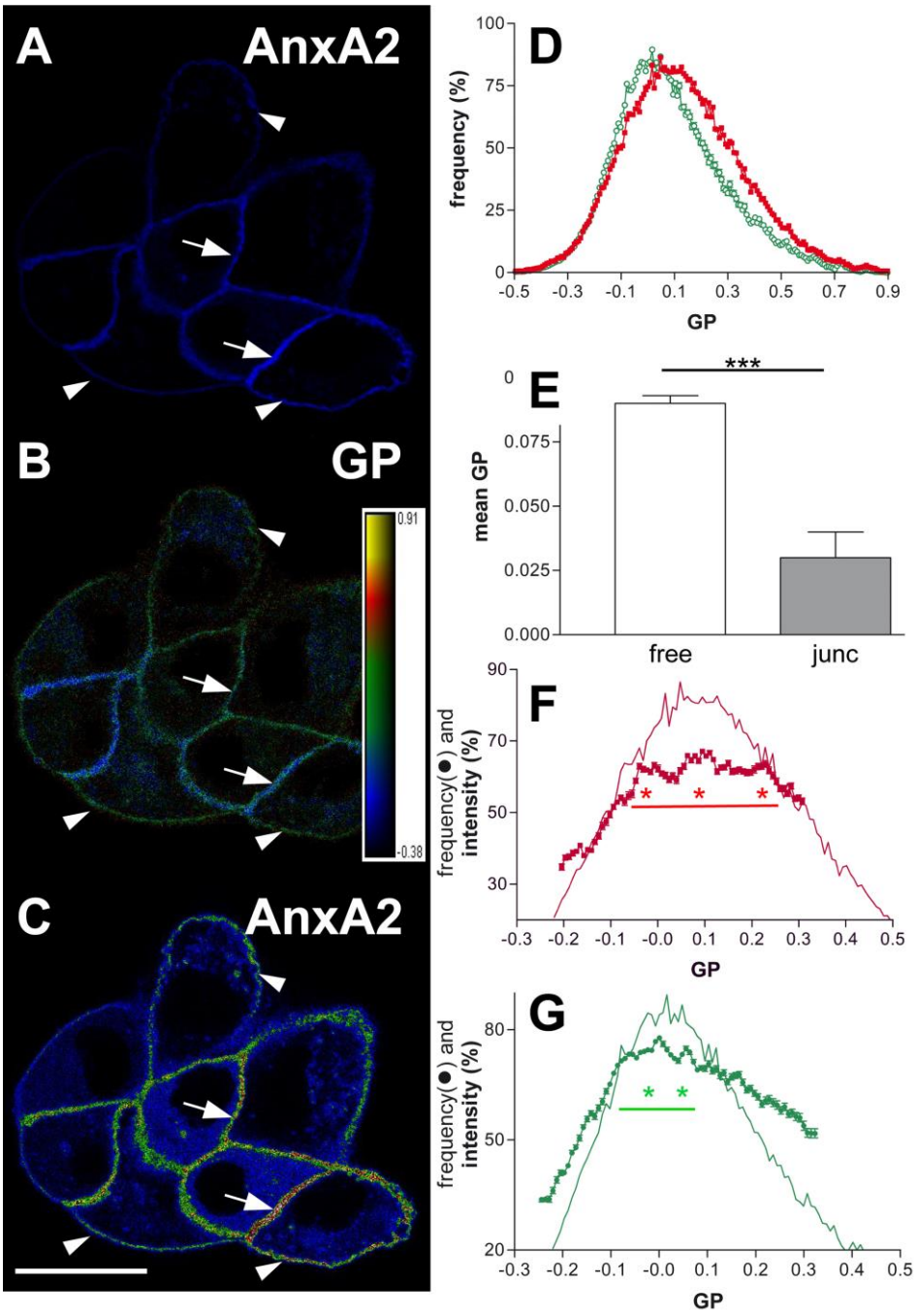

Fig. 3. GP distribution and AnxA2 intensity in MDCK cells. A) Fluorescent confocal image of AnxA2-GFP expressing cells. B) Corresponding GP values showing the membrane order gradient for Lo membranes (blue) and Ld membranes (yellow). C) AnxA2-GFP signal from (A) coded in a coloured gradient (LUT, 5 Ramps with ImageJ) to clearly show the correlation between AnxA2-GFP intensity and the GP values. Free membranes (arrowheads) and junctional membranes (arrows). D) GP distribution of free membranes (red squares ■) and junctional membranes (green circles ○). E) Mean peak of GP distribution of MDCK free and junctional (junc) membranes. F,G) correlation of AnxA2-GFP intensity and the membrane GP values for free membranes (F) and junctional membranes (G). Lines under the curves indicate the ranges of relative stronger AnxA2-GFP intensity and the stars the AnxA2-GFP intensity peaks. Mean ± SEM from 13 to 18 microscopy fields and 4 to 6 confocal planes. Each field contained several cells, *** $P < 0.0001$. Bar, 20 µm.

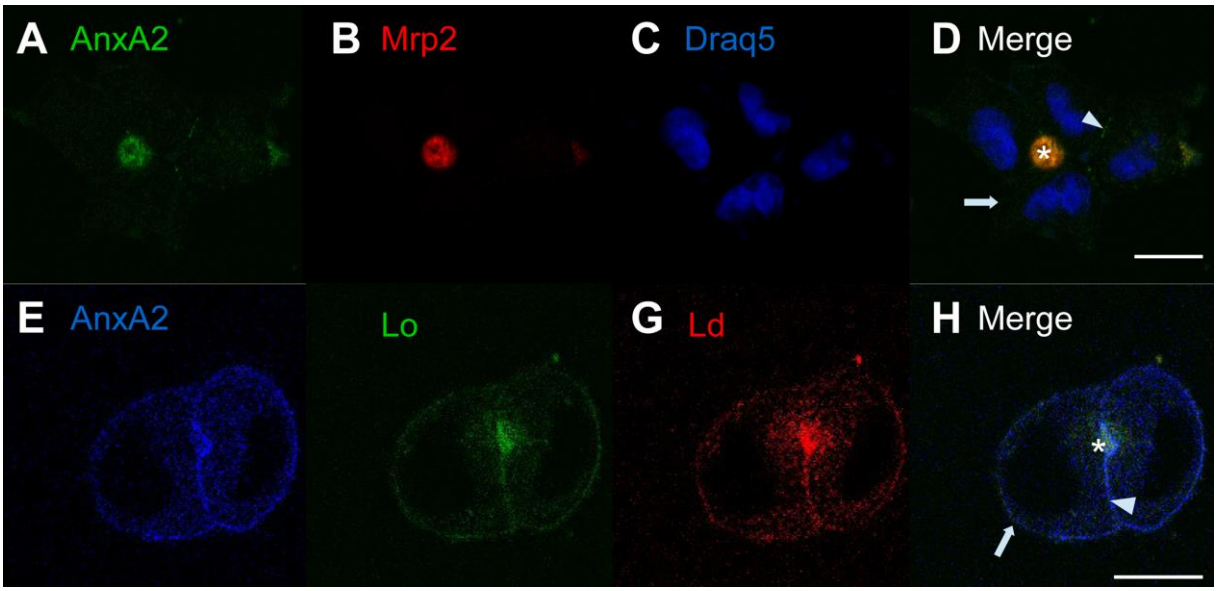

Fig. 4. AnxA2 expression in differentiated HepG2 cells. Confocal images of WT HepG2 (A-D) and AnxA2-GFP-expressing HepG2 cells (E-H). Immunofluorescence images for AnxA2 (A) and MRP2 (B). DRAQ5 (C) and merge image (D). AnxA2-GFP-expressing cells labelled with ANE. AnxA2-GFP (E), Lo contribution (F), Ld contribution (G) and merge (H). Free plasma membrane (arrow) junctional membranes (arrowhead) and canaliculi (*). Bars, 20 µm.

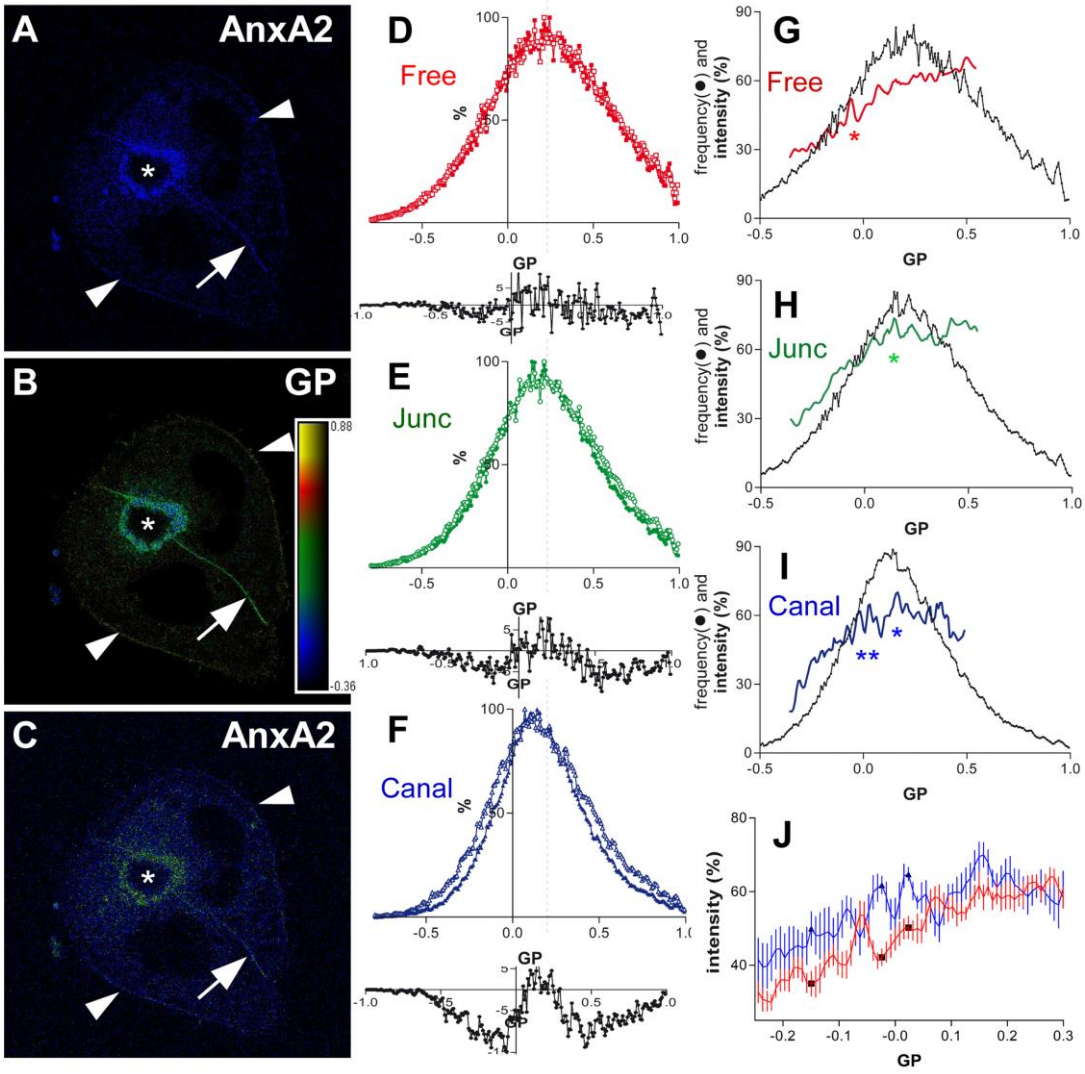

Fig. 5. GP distribution and AnxA2 intensity in HepG2 cells. A) Fluorescent confocal image of AnxA2-GFP expressing cells. B) Corresponding GP values showing the membrane order gradient with Lo membranes in blue and Ld membranes in yellow. C) AnxA2-GFP signal from (A) coded in a coloured gradient (LUT, 5 Ramps with ImageJ) for clearly show the correlation between AnxA2-GFP intensity and the GP values. Free membranes (arrowheads), junctional membranes (arrow) and canaliculi (*). GP distribution of free membranes (D), junctional membranes (E) and canalicular membranes (F), in WT (empty symbols □, ○, Δ) and AnxA2-GFP expressing cells (filled symbols ■, ●, ▲). For comparison, dotted line indicates the peak of junctional membranes (GP=0.2). The bottom part of (D-F) show the subtractions of GP distribution of AnxA2-GFP minus WT. (G) to (J) show the correlation of AnxA2-GFP intensity (coloured lines) as function of GP values of the membrane for free (G), junctional (H), and canalicular membranes (I). Stars (*) indicate specific AnxA2 expression increase. (J) Comparison of the AnxA2-GFP relative expression as a function of GP for free (red) and canalicular (blue) membrane regions. Some GP values are relatively enriched in AnxA2-GFP in canalicular membranes compared to free membranes (black points). Means from 12 to 38 microscopy fields containing 4 to 6 confocal planes from three independent experiments. The difference between free and canalicular points were statistically significant by unpaired two tailed t-test. Points; -0.15 P=0.014 (*), -0.024 P<0.0001 (***) and 0.024 P=0.002 (**).

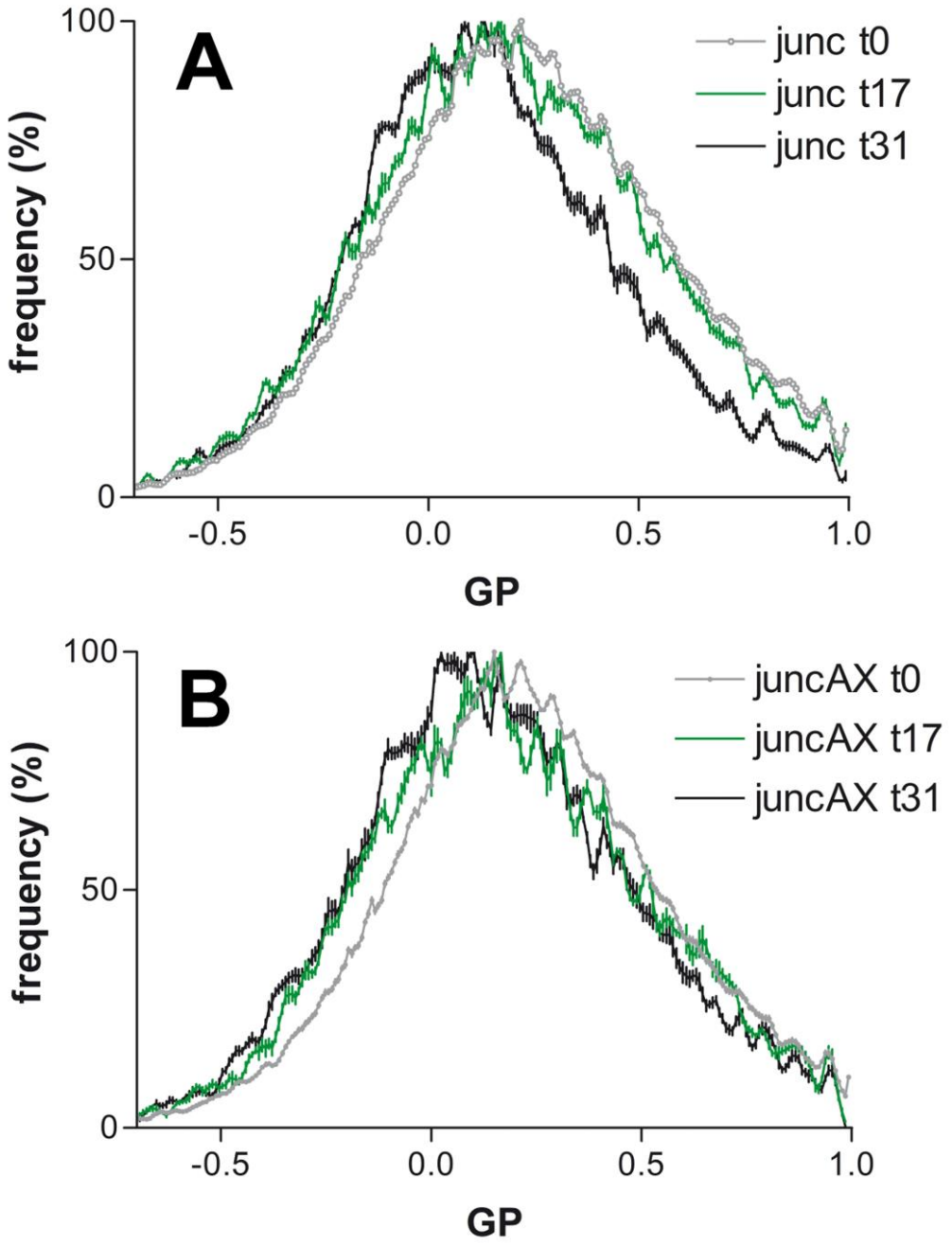

Fig. 6. GP distribution in HepG2 cells after ionomycin treatment. GP distribution of junctional membranes from WT cells (A) and AnxA2-GFP expressing cells (B) at different times after ionophore treatment. Before ionophore addition (t0) and at 17 and 31 minutes after ionophpre addition. Means from 5 to 9 microscopy fields containing several cells and 4 to 6 confocal planes.